Pergamon

Geochimica et Cosmochimica Acta, Vol. 65, No. 7, pp. 1025–1035, 2001

0016-7037/01 $20.00 + .00

PII S0016-7037(00)00587-1

The effect of growth phase on proton and metal adsorption by *Bacillus subtilis*

CHRISTOPHER J. DAUGHNEY,[1,*] DAVID A. FOWLE,[2] and DANIELLE FORTIN[1]

[1]Department of Earth Science, University of Ottawa, 140 Louis Pasteur, Ottawa, ON, K1N 6N5, Canada
[2]Great Lakes Institute for Environmental Research, University of Windsor, Windsor, ON, N9B 3P4, Canada

(*Received June* 7, 2000; *accepted in revised form October* 13, 2000)

Abstract—Several recent studies have applied surface complexation models to quantify metal adsorption by bacterial surfaces. Although these models can account for the effects of many abiotic variables (such as pH and ionic strength), to date, the effects of biotic variables (such as growth phase) have not been investigated. In this study, we quantify the effect of growth phase on surface site concentrations, deprotonation constants, and metal-binding constants by performing acid-base titrations and Cd and Fe(III) batch adsorption experiments using suspensions containing *Bacillus subtilis* cultured to exponential, stationary, and sporulated phase. For each type of surface site, concentrations and pK_a values describing deprotonation decrease as the cells move from exponential to stationary phase, but remain constant from stationary to sporulated phase. Due to the variations in site concentrations and deprotonation constants, Cd and Fe(III) binding constants are largest for stationary-phase cells and smallest for sporulated cells, even though cells in stationary phase adsorb roughly 5% to 10% less metal (per unit weight) than exponential-phase cells, and roughly 10% to 20% more metal than sporulated cells. These variations in surface complexation model parameters indicate that any attempt to predict proton or metal adsorption by bacteria must consider the growth phase of the population.

1. INTRODUCTION

The adsorption of metals by bacteria can influence a variety of geochemical processes. Due to their extremely high surface-area-to-volume ratio, and due to the presence of specific cell-wall functional groups with high affinities for dissolved metals, bacterial surfaces are very efficient metal sorbents (Beveridge and Murray, 1980; Beveridge et al., 1982; Gonçalves et al., 1987; Beveridge, 1989; Fein et al., 1997; Daughney and Fein, 1998a; Daughney et al., 1998; Fowle and Fein, 1999). Adsorption of metals by bacteria may affect mineral dissolution and precipitation (Beveridge et al., 1983; Konhauser et al., 1993; Fortin et al., 1997; Fortin and Ferris, 1998; Warren and Ferris, 1998), transport of metallic contaminants (Corapcioglu and Kim, 1995), and formation of some low-temperature ore deposits (Savvichev et al., 1986). Further, because metal adsorption affects the chemical and electric properties of the cell surfaces, it may also affect their ability to adsorb organics (Baughman and Paris, 1981; Daughney and Fein, 1998b; Fein and Delea, 1999) or to adhere to mineral surfaces (van Loosdrecht et al., 1989, 1990; Yee et al., 2000). In addition to the reactivity of their surfaces, it is their distribution and quantity that lead bacteria to influence so many important geochemical processes. Bacteria are found in almost all fluid-rock systems, including fresh and saline surface waters (Geesey et al., 1977; Harvey et al., 1982), groundwaters (Mahmood and Rama, 1993; Corapcioglu and Kim, 1995), deep-sea hydrothermal systems (Mandernack and Tebo, 1993; Baker et al., 1994), and deep sedimentary basins (Ghiorse and Wobber, 1989; Yakimov et al., 1995). Bacteria do not merely exist in these fluid-rock systems, they proliferate. For example, near-surface flow systems commonly contain 10^6 to 10^8 cells per gram of sediment (Chapelle, 1993). Bacteria are able to survive and metabolize in extreme conditions, having been isolated from environments with temperatures of less than 0°C and more than 90°C, from systems with pressures approaching 1000 atm, from waters with pH values less than 3 and more than 10, and from solutions many times more saline than seawater (Kushner, 1978). In natural environments, bacteria and their extracellular polysaccharides tend to coat mineral surfaces (Marshall, 1980; Harvey et al., 1982), such that they represent a significant fraction of the total surface area exposed to the aqueous phase. With their ubiquity and their ability to adsorb metals considered together, it becomes apparent that bacteria have the potential to influence the distribution and transport of mass in many fluid-rock systems.

Because metal adsorption by bacteria is such an important geochemical process, adequate predictive models are essential. Recently, several researchers have used surface complexation models to quantify the extent of proton and metal adsorption by bacteria (Gonçalves et al., 1987; Fein et al., 1997; Daughney and Fein, 1998a; Daughney et al., 1998; Warren and Ferris, 1998; Cox et al., 1999; Fein and Delea, 1999; Fowle and Fein, 1999; Fowle et al., 2000; Yee et al., 2000). These models use a thermodynamic stability constant (K) and mass action law to describe the adsorption of a certain dissolved species (e.g., Pb^{2+}, $CuOH^{+}$, etc.) by a particular type of surface functional group (e.g., carboxyl, phosphate, etc.). For example, the adsorption of Pb^{2+} by a deprotonated carboxyl group on the cell wall of *Bacillus subtilis* is described by the following chemical reaction and mass action law (Fein et al., 1997; Daughney and Fein, 1998a; Fowle and Fein, 1999):

$$RCOO^- + Pb^{2+} \leftrightarrow RCOOPb^+ \quad (1)$$

$$K = \frac{[RCOOPb^+]}{[RCOO^-]a_{Pb^{2+}}} \quad (2)$$

* Author to whom correspondence should be addressed (daughney@science.uottawa.ca).

where *R* represents the bacterial cell wall to which the functional group is attached, square brackets represent the concentrations of the enclosed surface species (moles per kg solution), and *a* represents the activity of the subscripted species. It is important to note that the above is just one of several important surface reactions in the Pb-*B. subtilis* system. With all relevant reactions taken into account, and with their corresponding stability constants corrected for the effects of surface charge and ionic strength, it becomes possible to predict the extent of metal adsorption that will occur, regardless of the concentration of metal, concentration of bacteria, pH, ionic strength, or system chemical composition. This point is well illustrated by Fowle and Fein (1999), who use a surface complexation model to effectively predict the competitive adsorption of Cd, Pb, and Cu in a system containing both *B. subtilis* and *B. licheniformis*, as sorbate-to-sorbent ratio and solution pH are varied.

Although existing surface complexation models can account for the effects of most, if not all, abiotic variables affecting metal-bacteria adsorption, the effects of biotic variables have not been considered. In existing models, the bacterial surfaces are assumed to have fixed concentrations of functional groups, each with a fixed stability constant. However, bacteria are living organisms, and their surface characteristics can vary with growth physiology and metabolic state (Kjelleberg and Hermansson, 1984; Stenström and Kjelleberg, 1985; McEldowney and Fletcher, 1986; Stenström, 1989; van Loosdrecht et al., 1990; Weiss et al., 1995).

Growth phase is a biotic variable that can affect metal adsorption by a bacterial population (see Tortora et al., 1995 for more detail on the phases of microbial growth). For example, Macaskie and Dean (1984) have found that Cd is most extensively adsorbed by *Citrobacter* when the cells are in mid-exponential phase, though they point out that this is likely related to changes in the chemistry of their experimental system. Chang et al. (1997) have reported that Pb is most extensively adsorbed by stationary phase *Pseudomonas aeruginosa*, and Cd is most extensively adsorbed by exponential phase cells, but adsorption of Cu is not affected by growth phase. Using four different species, Friis et al. (1986) found that U is most extensively adsorbed by populations when they are in stationary phase. Norberg and Persson (1984) and Shuttleworth and Unz (1993) have noted that adsorption is affected by the age of the cell culture, but they do not report growth phase. Although the effect of growth phase appears to be metal- and species-specific, to date, this has not been quantitatively investigated.

In this study, we investigate the effect of growth phase on the adsorption of H^+, Cd and Fe(III) by *B. subtilis*, a common soil bacterium. We perform acid-base titrations and batch Cd and Fe adsorption experiments, using bacterial populations cultured to exponential, stationary, and sporulated phase. In each case, we describe the experimental data by using surface complexation models, with the aim of quantifying any variation in the surface site concentrations and proton- and metal-binding constants associated with changing growth phase. Our objective is to determine a set of surface complexation model parameters that apply to each of the three growth phases, in order to facilitate geochemical modeling of complex natural systems.

2. METHODS

2.1. Growth Procedures

B. subtilis cells were obtained from T. J. Beveridge (University of Guelph, Ontario, Canada). The bacteria were precultured in 3-mL volumes of autoclaved (120°C for 20 min) trypticase soy broth (Becton Dickinson, Mountain View, CA, USA) containing 0.5 wt.% yeast extract (Becton Dickinson). After growing for 24 ± 0.1 h at 37°C, two of the 3-mL precultures were transferred to a 1-L volume of autoclaved broth, which was then placed on an orbital shaker (100 rpm) at 37°C. Optical densities of the cultures were measured at 600 nm during growth, in order to determine the time required to reach exponential and stationary phase. Sporulation was observed by optical microscopy. Based on the results of these observations (not shown), independent cultures of bacteria were harvested at 7.5 ± 0.1 h, 24 ± 0.1 h, and 48 ± 0.1 h, for mid-exponential, late stationary, and sporulated phase, respectively. In all cases, the cells were removed from the growth medium by centrifugation (6000 rpm, 10 min), rinsed three times in distilled, deionized (DDI) water (18 MΩ), soaked in 0.001 M ethylenediaminetetraacetic acid for 0.5 ± 0.05 h, then rinsed four times in 0.01 M $NaNO_3$ (the electrolyte used in the experiments). After each step in the wash procedure, the bacteria were pelleted by centrifugation (6000 rpm, 10 min) and the supernatant was discarded. This wash procedure was followed to strip the cell walls of metals that may have been present in the growth medium, and to leave the bacteria intact, viable, and in a resting state (Cox et al., 1999; Fein and Delea, 1999). Here, and in all the procedures described below, all plastic and glassware were sequentially soaked in 10% nitric acid and then in DDI water prior to use, after Cox et al. (1999).

2.2. Acid-Base Titrations

Within 15 min of the final rinse, a known weight (~40 g) of a suspension containing bacteria in 0.01 M $NaNO_3$ was placed in an air-tight polystyrene vessel. The pH was adjusted to roughly 3.5 by the addition of a weighed aliquot of standardized HNO_3, and the suspension was mixed with a magnetic stirrer and bubbled with CO_2-free N_2 for 30 min, in order to remove dissolved CO_2 from the suspension. The titrations were conducted in an up-pH direction, using a Radiometer TTT85/ABU80 autotitrator (Copenhagen, Denmark) with a Ross Sure-Flow combination electrode (Columbus, OH, USA). Standardized CO_2-free NaOH was used as the titrant, and the suspensions were mixed and bubbled with N_2 as described above. Following each addition of titrant, the pH of the suspension was recorded when a stability of 0.1 mV/s was obtained, after Fein et al. (1997) and Cox et al. (1999). A stability criterion of 0.02 mV/s was also investigated, but later discarded because it facilitated cell lysis at high pH. After the completion of each titration, the pH was again adjusted to roughly 3.5 by the addition of a weighed amount of HNO_3, and a second up-pH titration was conducted to evaluate the reversibility of proton adsorption. Using this experimental method, titrations of the electrolyte alone displayed a single inflection point, indicating that the system was free of CO_2, and replicate titrations of sodium acetate agreed with each other and with theoretical predictions, indicating that the method was precise and accurate. Titrations of three independently grown bacterial cultures were conducted for each of the three growth phases. In all cases, following the second up-pH titration, three weighed aliquots of the suspension were centrifuged at 6000 rpm for 1 h, the solutions were discarded, and the pellets were weighed, to determine the wet weight of bacteria present (after Fein et al., 1997). All weights reported in this paper refer to centrifuged weights, not to dry weights. For comparison to earlier work (e.g., reviews by Gadd, 1988; Volesky and Holan, 1995), we also determined the dry mass of bacteria by oven-drying (60°C) the centrifuged pellets to constant weight. We determined the ratio of wet to dry weight to be 10.2 ± 0.8 to 1, in good agreement with the value of 9.9 ± 1.1 to 1 reported by Fein and Delea (1999).

2.3. Metal Adsorption Experiments

Batch Cd adsorption experiments were conducted as a function of pH (2.3–8.0), solid-to-solution ratio, and growth phase. A homogeneous bacteria-Cd suspension was prepared in 0.01 $NaNO_3$ by adding

a known mass of bacteria (as described above) and 100 ppm Cd (in 0.01 $NaNO_3$/0.2% HNO_3) standard solution to a Teflon reaction vessel. Final Cd and bacterial concentrations ranged from 9.9 to 10.2 ppm and 3 to 8 g bacteria/L. Aliquots (10 mL) of the parent solution were transferred to polypropylene reaction vessels, and the pH of the suspension in each vessel was adjusted to the desired pH value by using small volumes of standardized HNO_3 and NaOH. The reaction vessels were placed on a rotating rack that provided gentle (20 rpm) end-over-end agitation for 2 h. Metal adsorption kinetics experiments in previous studies have demonstrated that 2 h is sufficient for adsorption equilibrium to occur (Fein et al., 1997; Fowle and Fein, 2000). The suspension was then filtered through a 0.1-μm nylon filter. Each filtrate was acidified and analyzed for aqueous metal content by Inductively Coupled Plasma Atomic Emission Spectrometry (ICP-AES).

The Fe adsorption experiments were conducted over a narrow pH range (2.4–3.0), as a function of Fe-to-bacteria ratio, in order to avoid precipitation of $Fe(OH)_3$. A bacterial suspension was prepared in 0.01 M $NaNO_3$, and three weighed aliquots were centrifuged for 1 h to determine the wet weight of bacteria per unit weight of suspension, as described above. Known weights (0.5–10 g) of this parent suspension were transferred to a series of reaction vessels, and diluted to a final weight of roughly 10 g with varying amounts of 0.01 M $NaNO_3$. A known weight of a 1000 ppm Fe solution was added to each reaction vessel to yield an initial Fe concentration of roughly 10 ppm, and the pH was adjusted with HNO_3 as required. Equilibration times and sampling techniques were identical to those described for the Cd experiments. The final concentration of dissolved Fe was determined by flame atomic absorption spectrophotometry. This experimental procedure was repeated by using two independently grown cultures at each of the three growth phases.

3. RESULTS AND DISCUSSION

3.1. Acid-Base Titrations

The experimental data, normalized to the wet weight of bacteria present, indicate that the buffering capacities of stationary and sporulated populations are very similar, but are much less than exponential-phase populations (Fig. 1). Note that: 1) we plot only every fourth data point for clarity, though we consider all data points in our modeling; and 2) the electrolyte display virtually no buffering in the pH range of our investigation. For each of the three growth phases, there is good agreement between the three individual titrations (of independently grown cultures), even though the bacterial concentrations varied (10–25 g/L). The stationary- and sporulated-phase titration data collected here agree very well with the best-fitting model of Daughney and Fein (1998a) (dashed curves, Fig. 1). In all cases, the titrations are completely reversible on the time scale of these experiments (<1 h; Fig. 2; data for stationary-phase populations are omitted for clarity).

We attempt to fit the experimental data with surface complexation models that assume that the observed buffering is due to the deprotonation of functional groups on the cell walls. The cell wall may display several different types of functional groups (e.g., carboxyl, phosphate, hydroxyl, amine, etc.), which we designate as L_1H, $L_2H \ldots L_nH$ in the following discussion. The deprotonation of the functional group L_nH can be expressed by the following chemical reaction and mass action law:

$$RL_nH^0 \leftrightarrow RL_n^- + H^+ \tag{3}$$

$$K_n = \frac{[RL_n^-]a_{H^+}}{[RL_nH^0]} \tag{4}$$

where R represents the cell wall to which the functional group is attached, K_n represents the stability constant describing deprotonation, square brackets represent the concentrations of the enclosed surface species (moles per kg solution), and a represents the activity of the subscripted species.

We use the computer program FITEXP to determine how many different types of functional groups are required to describe the experimental data, and to solve for their deprotona-

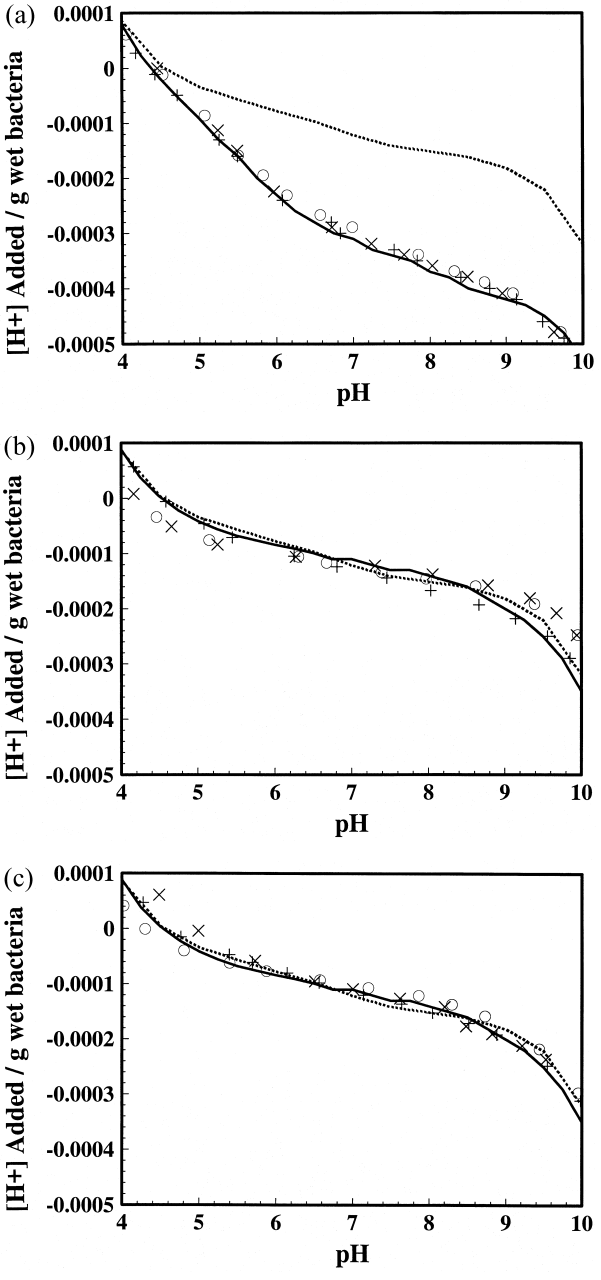

Fig. 1. Experimental data gathered during acid-base titration of *B. subtilis* cultured to a) exponential, b) stationary, and c) sporulated phase, normalized with respect to the wet weight of bacteria present. Different symbols represent different titrations conducted using independently grown cultures of bacteria. Solid lines represent best-fitting models. For exponential phase, model parameters are compiled in Table 2, row 1; for stationary and sporulated phase, model parameters are listed in Table 2, row 4. Dashed lines represent the best-fitting model of Daughney and Fein (1998a), for stationary-phase *B. subtilis.*

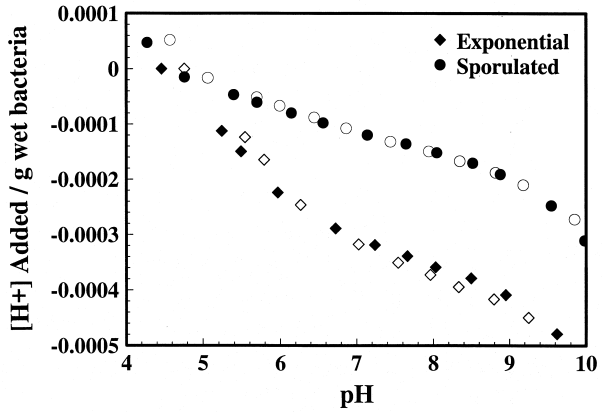

Fig. 2. Representative data gathered during acid-base titrations to test the reversibility of the proton adsorption-desorption reaction. Closed and open symbols of the same shape represent the first and second up-pH titrations, respectively. The reversibility of stationary-phase populations was also evaluated, but the data have been omitted for clarity.

tion constants and absolute concentrations. FITEXP is a form of FITEQL 2.0 (Westall, 1982a,b) modified by J. Lützenkirchen (Department of Inorganic Chemistry, Umeå University, Sweden; pers. commun., 1998) to allow simultaneous modeling of systems with different solid-to-solution ratios. Deprotonation constants are referenced to zero ionic strength by using the Davies equation, and to zero surface charge by using the constant capacitance double-layer model, with a surface area of 140 m^2/g and a capacitance of 8.0 F/m^2, after Fein et al. (1997). Surface site concentrations are expressed in moles per gram of wet bacteria. In all of our modeling, we optimize for the deprotonation constants and the site concentrations simultaneously. Equilibria describing the dissociation of water, the acid, the base, and the electrolyte are included in the models, with stability constants from Smith and Martell (1976). FITEXP calculates the error (Y) in the chemical mass balance equation as:

$$Y = \sum_i a_{ij} C_i - T_j \tag{5}$$

where the subscript i is used to represent any species and j is used to represent any component, and a, C, and T represent the applicable stoichiometric coefficient, free concentration, and total concentration, respectively. The overall variance $V(Y)$ thus provides a quantitative measure of the goodness of the model fit to the experimental data:

$$V(Y) = \frac{\sum_{P,Q} \left(\frac{Y}{s_Y}\right)^2}{n_P n_Q - n_R} \tag{6}$$

where the summation is performed over all data points P and all components Q for which both C and T are known. The standard deviation for Y (s_Y) is calculated by the propagation of experimental errors associated with the determination of C and T. The sum of squares is normalized with respect to the number degrees of freedom in the system, as determined by the data points (n_P), the number of components (n_Q), and the number of parameters being optimized (n_R). For systems containing a reactive surface, values of $V(Y)$ from 1 to 20 indicate a good fit to the data (Westall, 1982a,b), and in the authors' experience, values from 20 to 30 indicate an acceptable fit to the data.

We begin by modeling each of the nine titrations individually. For each titration, it is possible to obtain a good fit to the data by using a model with three different types of surface functional groups, with $V(Y)$ less than 20 in most cases (Table 1). The low values of $V(Y)$ indicate that the three-site model provides sufficient complexity to describe the experimental data. Adding a fourth site does not decrease $V(Y)$, showing that the additional site is not warranted by the data, and models that consider only one or two types of cell-wall functional groups yield excessively large values of $V(Y)$. Thus one-, two-, and four-site models are not considered further. Our selection of the three-site model is in agreement with Fein et al. (1997). By using discrete affinity spectra, Cox et al. (1999) have described proton adsorption by *B. subtilis* with a five-site model, but they point out that models with fewer sites would also be possible. Based on the deprotonation constants determined here (Table 1), relative to those of short-chain organic acids, it is likely that L_1H and L_2H represent carboxyl and phosphate functional groups, respectively, as described previously (Fein et al., 1997;

Table 1. Model parameters describing individual acid-base titrations of *B. subtilis*.

Phase[a]	No[b]	pK_1[c]	pK_2	pK_3	C_1[d]	C_2	C_3	$V(Y)$[e]
Exp	1	5.33	7.18	9.30	32.1	8.00	15.6	9.9
	2	5.24	6.96	9.26	28.7	11.5	14.2	17.1
	3	5.41	7.39	9.33	34.6	9.30	13.6	26.4
Stn	1	4.72	6.43	8.02	6.04	1.84	3.95	13.5
	2	4.87	6.33	8.19	9.26	5.55	7.40	9.7
	3	4.81	6.70	9.36	5.05	5.66	7.16	8.5
Spr	1	4.76	6.72	9.04	11.6	7.50	16.0	26.7
	2	4.91	6.65	9.14	5.88	4.68	12.9	10.7
	3	4.77	6.93	9.19	10.1	6.63	15.5	6.0

[a] Growth phase of the bacterial population (Exp = exponential, Stn = stationary, Spr = sporulated).
[b] Titrations were performed on three independently grown cultures of bacteria.
[c] Negative logarithm of the stability constant describing deprotonation of the subscripted surface site (1 = carboyxl, 2 = phosphate, 3 = amine), referenced to zero ionic strength and zero surface charge.
[d] Concentration of the subscripted surface site, in $x\ 10^{-5}$ mol/g wet bacteria.
[e] Variance calculated by FITEXP.

Table 2. Average[a] model parameters describing acid-base titrations of *B. subtilis*.

Reference	Phase[b]	pK_1[c]	pK_2	pK_3	C_1[d]	C_2	C_3
This study[e]	Exp	5.33 ± 0.1	7.18 ± 0.3	9.30 ± 0.6	31.8 ± 3.9	9.60 ± 2.6	14.5 ± 2.2
This study	Stn	4.80 ± 0.1	6.49 ± 0.3	8.52 ± 0.6	6.78 ± 3.9	4.35 ± 2.6	6.17 ± 2.2
This study	Spr	4.81 ± 0.1	6.77 ± 0.3	9.12 ± 0.6	9.19 ± 3.9	6.27 ± 2.6	14.8 ± 2.2
This study[f]	Stn + Spr	4.81 ± 0.1	6.62 ± 0.3	8.82 ± 0.6	7.99 ± 3.9	4.54 ± 2.6	10.5 ± 2.2
Fein et al. (1997)	Stn	4.82 ± 0.1	6.9 ± 0.5	9.4 ± 0.6	12 ± 2	4.4 ± 0.3	6.2 ± 0.4
Daughney and Fein (1998a)	Stn	4.65 ± 0.4	6.16 ± 0.6	9.80 ± 0.8	6.72 ± 1.8	9.68 ± 4.0	53.6 ± 42

[a] Average model parameters from Table 1, and from other references, with corresponding 2σ errors calculated by ANOVA.
[b] Growth phase of the bacterial population (Exp = exponential, Stn = stationary, Spr = sporulated).
[c] Negative logarithm of the stability constant describing deprotonation of the subscripted surface site (1 = carboyxl, 2 = phosphate, 3 = amine), referenced to zero ionic strength and zero surface charge.
[d] Concentration of the subscripted surface site, in $x\ 10^{-5}$ mol/g wet bacteria.
[e] These average model parameters are used to plot the exponential-phase model curve in Figure 1.
[f] These average model parameters are used to plot both the stationary- and sporulated-phase model curves in Figure 1.

Daughney and Fein, 1998a; Daughney et al., 1998; Cox et al., 1999). L_3H may represent a type of hydroxyl functional group, as suggested by Fein et al. (1997), or an amine structure, as suggested by Cox et al. (1999). As pointed out by Cox et al. (1999), amine sites are abundant on the cell wall of *B. subtilis*, but hydroxyl sites with $8 < pK < 10$ (phenols) are not. Hereafter, L_1H, L_2H, and L_3H are referred to as carboxyl, phosphate, and amine sites, and are represented in the text by $RCOOH$, RPO_4H, and RNH_2, respectively. As discussed below, it is possible to further constrain the chemistry of these surface sites by comparing their metal-binding constants to those describing metal complexation by short-chain organic acids.

We find that the model deprotonation constants and site concentrations differ slightly between independent titrations, even for a single growth phase (Table 1). Errors associated with the experimental method were evaluated during replicate sodium acetate titrations, and were found to be ± 0.05 in the pK value and $\pm 2\%$ in the ligand concentration. Errors associated with weighing the bacteria affected the model pK values by less than ± 0.005, but affected the model site concentrations by $\pm 4\%$. These errors cannot account for the all of the variation in the model parameters compiled in Table 1. We therefore conclude that these variations represent differences in the surface properties of the individual cultures of the bacteria. Thus, for each of the three growth phases, we model the three independent titrations simultaneously to determine a single set of best-fitting model parameters (Table 2).

We also conduct a single-factor analysis of variance (ANOVA) to determine if, and at what confidence intervals, the average model parameters differ between the three growth phases (Table 3). We first conduct an F-test, and find that each model parameter has a statistically distinct average value for each of the three growth phases. Next, we compare the average model parameters between the three growth phases. We apply a two-standard-deviation threshold, such that a confidence interval of 0.95 or more indicates that the two averages being compared are statistically different, whereas a confidence interval of less than 0.95 indicates that they are not. By using this threshold confidence interval, we find that the majority of model parameters from the stationary and sporulated populations are the same. In contrast, the majority of exponential-phase model parameters are statistically different from those of either the stationary- or sporulated-phase populations. The ANOVA thus provides a quantitative affirmation of the visual trends shown in Figure 1. We also use the ANOVA to determine the 2σ errors corresponding to the average model parameters (Table 2).

Based on the statistical analysis of the average parameters, it is reasonable to model the stationary- and sporulated-phase populations simultaneously. Thus, we develop a single set of best-fitting model parameters applicable to both growth phases (Table 2), and we compare the model fit to the experimental data in Figure 1b,c. The exponential-phase populations require

Table 3. Confidence intervals at which average model parameters can be considered statistically different, based on a single-factor ANOVA.

Comparison[a]	pK_1[c]	pK_2	pK_3	C_1[d]	C_2	C_3
Exp vs. Stn phase (this study)	0.99	1.00	0.97	1.00	0.96	1.00
Exp vs. Spr phase (this study)	0.99	0.98	0.93	1.00	0.92	0.57
Stn vs. Spr phase (this study)	0.53	0.94	0.68	0.77	0.79	0.99
Stn phases (this study vs. Fein et al., 1997)	0.61	0.91	0.90	0.99	0.51	0.51
Stn phases (this study vs. Daughney and Fein, 1998a)	0.73	0.81	0.93	0.51	0.95	0.96

[a] Comparisons are between the average model parameters (listed in Table 2) for the three different growth phases in this study (Exp = exponential, Stn = stationary, Spr = sporulated), and between the stationary-phase parameters from this and other studies.
[b] Number of degrees of freedom.
[c] Confidence intervals at which the average deprotonation constants can be considered different.
[d] Confidence intervals at which the average concentrations of the subscripted surface sites can be considered different.

a different set of best-fitting model parameters, which are compiled in Table 2 and used to plot the model curve in Figure 1a.

We also compare the stationary-phase-model parameters determined in this study to those of Fein et al. (1997) and Daughney and Fein (1998a) (Tables 2 and 3). These authors also conducted acid-base titrations of *B. subtilis* in $NaNO_3$ (Fein et al., 1997 used 0.1 M, Daughney and Fein, 1998a used 0.01 M). These authors did not monitor growth phase, but they did consistently harvest their cultures after 24 h. We used the same growth protocol as these two earlier studies, and so it is reasonable to assume that their data apply to stationary-phase populations. By using ANOVA to compare the average model parameters, we find that the majority differ at a confidence interval of 0.95 or less, and so should be considered indistinct. This is to be expected, as the growth conditions and experimental methods are the same. Model predictions of proton adsorption by stationary-phase populations—based on parameters from this study, from Fein et al. (1997) or from Daughney and Fein (1998a)—are all very similar.

The effect of growth phase on proton adsorption is likely related to changes in the structure and composition of the cell wall, which in turn are affected by the changing chemistry of the growth medium. McLean and Beveridge (1990) have found that the nature and degree of peptidoglycan cross-linkage in the *B. subtilis* cell wall can change with the chemistry of the growth medium, and this may potentially alter the number of carboxylic-binding sites on the cell wall. These authors have also pointed out that as phosphate is depleted from the growth medium, *B. subtilis* cells walls are depleted of teichoic acid and enriched in teichuronic acid, which may affect the number of phosphate-binding sites. These studies indicate that the chemistry of the medium changes as the population grows, and as a result the cell-wall composition and its capacity to adsorb protons can also vary with growth stage.

There are two other ways in which growth phase may affect proton adsorption, which, although not pertinent to this study, are worthy of mention. First, when cells are metabolically active, a membrane-induced proton motive force continuously supplies H^+ to the cell wall, such that the cells may adsorb less H^+ from solution (Urrutia et al., 1992; Kemper et al., 1993). This is not applicable to our work because our washing procedure ensures that the cells are metabolically inactive. Second, if the cells are not removed from the growth medium, changes in its chemistry may affect proton adsorption by way of chemical competition with, for example, extracellular polysaccharides, metabolic waste products, or cell-wall fragments. Again, because we removed the cells from the growth medium before conducting our experiments, the chemical speciation of the suspension was known and constant.

We conclude that all changes in proton adsorption observed in this study are due to changes in the structure and composition of the cell wall. We suggest that an abundance of nutrients available to exponential-phase cells allows them to develop cell wall structures with high concentrations of anionic sites. As the concentration of nutrients is depleted, the population enters stationary phase, and cell wall structures with lower densities of anionic functional groups are favored. Note also that the deprotonation constant of any type of functional group depends, to some extent, on the structure of the cell wall to which it is attached (Daughney et al., 1998). We observed significant changes

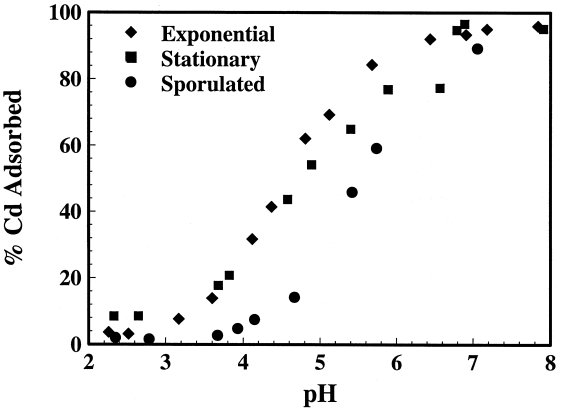

Fig. 3. Adsorption of Cd (10 ppm total concentration) by *B. subtilis* (5.0 g wet bacteria/l) as a function of growth phase and pH. Each data set represents an independently grown culture of bacteria.

in each of the deprotonation constants (Table 2) as the cells pass from exponential to stationary phase, providing further evidence that the cell wall structure was changing. The transition from stationary to sporulated phase was not accompanied by a significant change in the chemistry of the medium and, hence, the concentrations and deprotonation constants of the cell wall functional groups remained relatively constant. We recommend that proton adsorption by exponential-phase populations of *B. subtilis* be modeled using the "Exp" parameters compiled in row 1 of Table 2, and that proton adsorption by either stationary or sporulated populations be modeled using the "Stn + Spr" parameters in row 4 of Table 2.

3.2. Cd Adsorption Experiments

In the range $4 < pH < 7$, the amount of Cd adsorbed by a given mass of exponential-phase cells is roughly 5 to 10% more than that adsorbed by stationary-phase cells, which in turn is roughly 10 to 20% more than that adsorbed by sporulated cells (Fig. 3). In addition, the amount of Cd adsorbed increases with increasing pH and with increasing bacteria-to-metal ratio (Figs. 3 and 4). All of the solutions were undersaturated with respect to solid-metal phases, and metal adsorption by the apparatus was negligible, so the observed changes in aqueous metal concentration can be attributed entirely to cell-wall adsorption. Our experimental data are in good agreement with earlier studies (Fein et al., 1997; Daughney et al., 1998; Daughney and Fein, 1998a; Fein and Delea, 1999; Fowle and Fein, 1999).

We use FITEXP to determine site-specific stability constants describing Cd adsorption by the cell walls, for all pH values and bacteria-to-metal ratios (Table 4). We consider models invoking metal adsorption onto either the carboxyl sites alone (one-site model), or onto both the carboxyl and phosphate sites together (two-site model), and we consider only the 1 : 1 stoichiometry, after Fein et al. (1997), Daughney and Fein (1998a), Daughney et al. (1998), Fein and Delea (1999), and Fowle and Fein (1999). In our modeling of the exponential-phase data, we use the "Exp" parameters listed in Table 2, row 1; when modeling either stationary- or sporulated-phase data, we use the "Stn + Spr" parameters in Table 2, row 4. Equilibria describing Cd hydrolysis are included in our models, with stability con-

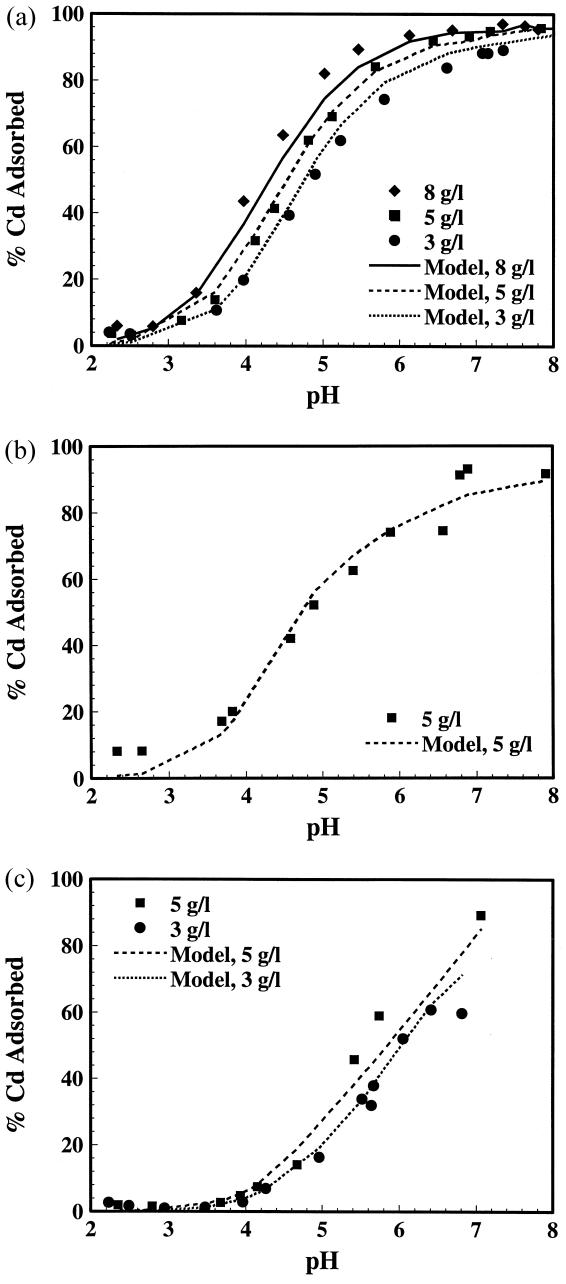

Fig. 4. Adsorption of Cd (10 ppm total concentration) by *B. subtilis* cultured to a) exponential, b) stationary, and c) sporulated phase, as a function of pH and wet weight of bacteria present. Model curves for exponential phase cells assume adsorption onto the carboxyl sites alone (Table 4, row 1); curves for stationary and sporulated phase cells assume adsorption onto carboxyl and phosphate sites (Table 4, row 2). Each data set represents an independent culture of bacteria.

stants taken from Baes and Mesmer (1976) and Smith and Martell (1978).

For each of the three growth phases, we first model data from the independently grown cultures separately, and then we model data from all the cultures simultaneously. As is the case for the titration models, for each growth phase, we find that the model parameters differ slightly between independently grown cultures of bacteria. These differences reflect either true variations in the surface properties of the individual cultures or uncertainties in the weight of bacteria present. Thus, for each of the three growth phases, we determine the best-fitting parameters by modeling all of the data simultaneously, but we model data from the independently grown cultures separately for ANOVA, to determine 2σ errors (Table 4).

Adsorption of Cd by exponential-phase *B. subtilis* is best described by a one-site model, whereas Cd adsorption by stationary- and sporulated-phase populations are best described by two-site models (Table 4, Fig. 4). At first, this is surprising, because the adsorption edges for the different growth phases occur over roughly the same pH range. However, the fit of each model is controlled, in part, by the deprotonation constants assumed to apply. The exponential-phase adsorption edge occurs over the pH range in which the carboxyl sites on exponential-phase cells are actively deprotonating ($pK_1 = 5.33$), but the phosphate sites are not ($pK_2 = 7.18$), and thus a one-site model fits the data well. In this same pH range, both the carboxyl ($pK_1 = 4.81$) and the phosphate sites ($pK_2 = 6.62$) on stationary phase and sporulated cells are actively deprotonating, and thus two-site models provide an improved fit to the data. In addition, the fit of each model is controlled by the assumed concentrations of surface sites, relative to the total concentration of the metal. The concentration of carboxyl sites on exponential phase cells is significantly greater than the concentration of the metal, and so a one-site model can account for 100% metal adsorption. In contrast, the concentration of carboxyl sites on the stationary and sporulated cells is less than the concentration of the dissolved metal, and so to account for 100% adsorption, an additional site must be included in the model.

In selecting a one-site model to describe metal adsorption by exponential-phase cells, but two-site models for stationary- and sporulated-phase cells, we are implying that the growth phase affects the surface properties of the cells, which in turn control the mechanism and extent of metal adsorption. Several previous studies have reported that the composition and structure of the cell wall influence electronegativity and metal binding. For example, Butter et al. (1998) have found that Cd uptake by *Streptomyces* is linearly related to the teichoic acid content of the cell wall, with scatter in the relationship reflecting the ability of other cell-wall components to bind the metal. By chemically modifying or removing certain structures in the *B. subtilis* cell wall, Beveridge and Murray (1980) reported that carboxyl structures in peptidoglycan dominate the adsorption of most cations, with binding by carboxyl and phosphate structures in teichoic acid of lesser importance. In a similar study using *B. licheniformis*, Beveridge et al. (1982) reported a more even distribution of metals between the peptidoglycan, teichoic acid, and teichuronic acid components of the cell wall. In a study comparing metal adsorption by *B. subtilis* and *B. licheniformis*, Daughney et al. (1998) found a strong correlation between the stability constants describing proton and metal adsorption to particular surface sites on the two species, which they concluded resulted from uniform compositional differences in the cell walls.

Although both proton adsorption and metal adsorption are both affected by growth phase, the relation between them is not straightforward. If the extent of metal adsorption could be predicted from the extent of proton adsorption, then (at a given

Table 4. Model parameters describing adsorption of Cd(II) by *B. subtilis*.

		Exponential phase			Stationary phase			Sporulated phase		
No.	Model reaction(s)[a]	log K[b]	2σ[c]	$V(Y)$[d]	log K[b]	2σ[c]	$V(Y)$[d]	log K[b]	2σ[c]	$V(Y)$[d]
1	$Cd^{2+}+RCOO^{-}\leftrightarrow RCOOCd^{+}$	3.52	0.2	7.1	3.72	0.2	16	3.25	0.2	32
2.	$Cd^{2+}+RCOO^{-}\leftrightarrow RCOOCd^{+}$	No convergence[e]			3.62	0.5	11	2.89	0.5	7.3
	$Cd^{2+}+\ RPO_4^{-}\leftrightarrow\ RPO_4Cd^{+}$				4.11			3.98	0.7	

[a] Reactions used to model experimental data; some models include two reactions.
[b] Logarithm of the stability constant for the corresponding reaction, referenced to zero ionic strength and zero surface charge.
[c] 2σ error for the corresponding stability constant, calculated by ANOVA.
[d] Variance calculated by FITEXP.
[e] Indicates severe misfit between the model and the experimental data.

pH and bacteria-to-metal ratio) we would expect exponential phase cells to adsorb more metal than either stationary or sporulated cells, in agreement with our data. However, we would also expect stationary and sporulated cells to adsorb identical amounts of metal, in contradiction to our data. We use ANOVA to assess the significance of the variation in the average Cd-carboxyl stability constants, in view of their corresponding 2σ errors. We find that: 1) the exponential-phase and stationary-phase values differ at a confidence interval of 0.74; and 2) the stationary- and sporulated-phase values differ at a confidence interval of 0.94. This analysis indicates that the magnitude of the Cd-carboxyl stability constant does not change significantly from exponential to stationary phase, but does change significantly from stationary to sporulated phase. This trend is different from that of the deprotonation constants, which change significantly from exponential to stationary phase, and then remain constant from stationary to sporulated phase. In explanation of this discrepancy, we note that the exosporium and spore coat of *B. subtilis* endospores are comprised of complex layers of protein, which could display proton accessible sites that are not readily accessible to metal cations. However, this hypothesis is speculative and remains to be verified by experimentally examining the reactivity of the endospore components.

Finally, we note that, in some cases, it is possible to further constrain the chemistry of the bacterial surface sites by comparing their metal binding constants to those describing metal complexation by short-chain organic acids. In all cases, the magnitudes of the Cd-carboxyl stability constants compiled in Table 4 are in good agreement with stability constants describing Cd complexation by carboxylic acids (e.g., oxalic acid, log $K = 3.9$; malonic acid, log $K = 3.2$; Martell and Smith, 1977), supporting the hypothesis that carboxylates are involved in Cd adsorption by *B. subtilis*. Several other metals display a similar agreement between the stability constants describing their adsorption to, and complexation by, carboxyl structures (Fein et al., 1997; Daughney et al., 1998; Fowle et al., 2000), further implicating the importance of these surface sites in metal binding by bacteria. The Cd-phosphate stability constants in Table 4 are also in general agreement with stability constants describing metal complexation by phosphonic acids (for most metals $2 < \log K < 6$, though few Cd-binding constants have been determined; Martell and Smith, 1977). Cd adsorption was not investigated at pH greater than 8, so we cannot perform the same type of correlation for the amine sites.

3.3. Fe Adsorption Experiments

The amount of Fe adsorbed by a given mass of exponential-phase cells is roughly 5 to 10% more than that adsorbed by stationary-phase cells, which in turn is roughly 10 to 20% more than that adsorbed by sporulated cells, and the amount of Fe adsorbed increases with increasing bacteria-to-metal ratio (Fig. 5). For each growth phase, independently grown cultures adsorb slightly different amounts of Fe under otherwise identical conditions. The Fe and Cd adsorption data thus show very similar trends. We are not able to assess the effect of pH on Fe adsorption, because the experiments were conducted over a narrow pH range (note that the pH of the experimental solutions did vary slightly, and although we take this into account in our modeling, it gives rise to some of the scatter visible in Fig. 5). Again, all of the experimental solutions were undersaturated with respect to solid phases, and Fe adsorption by the apparatus is negligible, so we attribute the observed changes in aqueous Fe concentration entirely to cell-wall adsorption. Our experimental data are in general agreement with the Fe adsorption data of Warren and Ferris (1998).

For each of the three growth phases, we use FITEXP to determine a single set of site-specific stability constants describing Fe adsorption by the cell walls, for all pH values and bacteria-to-metal ratios (Table 5). All of our models consider

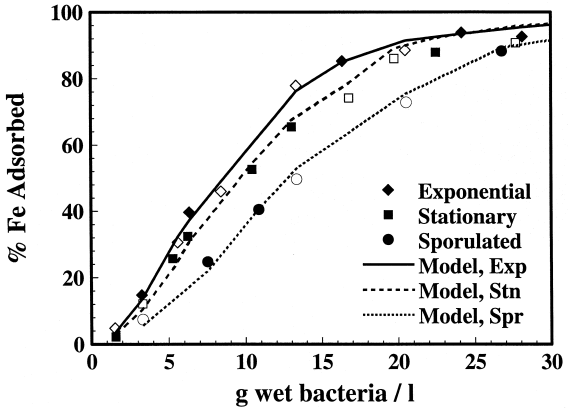

Fig. 5. Adsorption of Fe(III) (10 ppm total concentration) by *B. subtilis* (pH < 3) as a function of growth stage. Open and closed symbols of the same shape apply to two independent cultures of bacteria. Model curves assume the formation of a $(RCOO)_2Fe^{3+}$ surface complex (Table 5, row 3).

Table 5. Model parameters describing adsorption of Fe(III) by *B. subtilis*.

		Exponential phase			Stationary phase			Sporulated phase		
No.	Model reaction(s)[a]	log K[b]	2σ[c]	$V(Y)$[d]	log K[b]	2σ[c]	$V(Y)$[d]	log K[b]	2σ[c]	$V(Y)$[d]
1	$Fe^{3+} + RCOO^- \leftrightarrow RCOOFe^{2+}$	5.34	0.1	80	5.41	0.1	67	5.27	0.1	61
2.	$FeOH^{2+} + RCOO^- \leftrightarrow RCOOFeOH^+$	4.99	0.1	46	4.93	0.1	25	4.77	0.1	16
3.	$Fe^{3+} + 2RCOO^- \leftrightarrow (RCOO)_2Fe^+$	10.48	0.1	2.2	10.91	0.1	5.0	10.56	0.1	2.6
4.	$FeOH^{2+} + 2RCOO^- \leftrightarrow (RCOO)_2FeOH^0$	10.49	0.1	3.1	10.49	0.1	9.8	10.13	0.1	6.4
5.	$Fe^{3+} + 3RCOO^- \leftrightarrow (RCOO)_3Fe^0$	16.41	0.2	21	16.62	0.2	28	16.01	0.2	19
6.	$FeOH^{2+} + 3RCOO^- \leftrightarrow (RCOO)_3FeOH^-$	16.10	0.2	21	16.23	0.2	31	15.60	0.2	23
7.	$Fe^{3+} + RCOO^- \leftrightarrow RCOOFe^{2+}$	4.41	0.5	1.6	4.65	0.5	3.6	4.53	0.5	1.1
	$Fe^{3+} + 2RCOO^- \leftrightarrow (RCOO)_2Fe^+$	10.77	0.2		10.79	0.2		10.43	0.2	
8.	$FeOH^{2+} + RCOO^- \leftrightarrow RCOOFeOH^+$	4.28	0.3	1.6	4.52	0.3	5.4	4.41	0.3	1.8
	$FeOH^{2+} + 2RCOO^- \leftrightarrow (RCOO)_2FeOH^0$	10.37	0.2		10.2	0.2		9.81	0.2	

[a] Reactions used to model experimental data; some models include two reactions.
[b] Logarithm of the stability constant for the corresponding reaction, referenced to zero ionic strength and zero surface charge.
[c] 2σ error for the corresponding stability constant, calculated by ANOVA.
[d] Variance calculated by FITEXP.

adsorption by the carboxyl sites alone, because the experiments were conducted at low pH, where only the carboxyl sites are likely to be deprotonating. The experiments were conducted over the pH range in which Fe^{3+} is hydrolyzed to $Fe(OH)^{2+}$, and so we consider both of these species as potential sorbates. Finally, the experiments were conducted as a function of bacteria-to-metal ratio, so we consider the formation of surface complexes with various carboxyl-to-Fe stoichiometries. As described above, for each growth phase, we first model data from the two independently grown cultures separately, and then we model data from both simultaneously. We use the latter to determine a single set of best-fitting model parameters, and we use the former, in conjunction with ANOVA, to determine their 2σ errors. Again, we use the "Exp" parameters (Table 2, row 1) when modeling exponential-phase data and the "Stn + Spr" parameters (Table 2, row 4) when modeling either stationary- or sporulated-phase data. Equilibria describing Fe hydrolysis are included in our models, with stability constants taken from Langmuir (1997).

Several of the models provide good fits to the experimental data, and without additional information, we are unable to unequivocally identify the best-fitting model. Nonetheless, we favour the model considering the formation of the $(RCOO)_2Fe^+$ surface complex (Table 5, model 3) because: 1) it provides uniformly low values of $V(Y)$ for each of the three growth phases; 2) it is chemically reasonable, because a significant fraction of the dissolved Fe exists as Fe^{3+} in our experimental solutions; 3) the bacteria-to-metal ratio is high, such that the concentration of carboxyl sites exceeds the concentration of Fe, potentially favoring the formation of a bidentate surface complex; and 4) the magnitude of the stability constant is comparable to those describing formation of bidentate Fe complexes with short-chain carboxylic acids (acetic acid, log $K = 6.5$; oxalic acid, log $K = 13.6$; Martell and Smith, 1977). This model is compared to the experimental data in Figure 5.

Even though we cannot identify the best-fitting model, it is instructive to compare the values of the stability constant between the three growth phases. For example, for the $(RCOO)_2Fe^{3+}$ model, the values of the stability constant are all similar, but based on their associated uncertainties, can be considered statistically different (the exponential- and stationary-phase values differ at a confidence interval of 0.95; the stationary- and sporulated-phase values differ at a confidence interval of 0.94). Note that although the stability constant for the $(RCOO)_2Fe^{3+}$ reaction is largest for bacteria in stationary phase and smallest for bacteria in exponential phase, the amount of Fe adsorbed per unit weight of bacteria follows the trend exponential > stationary > sporulated phase (Fig. 5), because the concentrations of binding sites, and the deprotonation constants for these sites, vary between the growth phases. We suggest that the differences in the stability constant result from differences in cell wall structure between the growth phases. Our experimental methods do not permit us to probe the structure and composition of the cell wall directly, but we can point out that the relationship between growth phase, cell-wall structure, proton adsorption, and Fe adsorption is complex. Specifically, exponential-phase cells have the highest affinity for protons, but the lowest affinity for Fe. Stationary- and sporulated-phase cells display similar proton-binding capacities, but the former adsorb slightly more Fe than the latter.

4. CONCLUSIONS

In this study, we demonstrate that growth phase must be considered in surface complexation modeling of proton and metal adsorption by *B. subtilis*. Cells in exponential phase display roughly four times more carboxyl sites, twice as many phosphate sites, and 1.5 times as many amine sites (per unit weight) as cells in either stationary or sporulated phase. The pK values describing deprotonation of these functional groups are all roughly 0.5 log units larger for cells in exponential phase, compared to those for cells in either stationary or sporulated phase. Site concentrations and deprotonation constants for stationary- and sporulated-phase cells are statistically identical. Growth phase also affects metal adsorption by *B. subtilis*, with exponential-phase cells adsorbing more Cd and Fe(III) than stationary-phase cells, which in turn adsorb more than sporulated cells. Even with changes in the site concentrations and deprotonation constants taken into account, modeling metal adsorption by the three different growth phases requires three different sets of metal binding constants, and in the case of Cd,

different adsorption reactions altogether. Although we do not examine the cell wall structure directly, abundant literature evidence suggests that the relationship between adsorption behavior and growth phase is related to changes in cell-wall structure in response to changes in the chemistry of the growth medium.

Although the results of this study have profound implications for modeling metal adsorption by bacteria, a great deal more information is required before it is possible to accurately predict the fate of metals in bacteria-bearing fluid-rock systems. First, the effect of growth phase on metal adsorption by other species of bacteria must be investigated. Certainly, if other species of bacteria behave similarly to *B. subtilis*, accurate prediction of metal-bacteria adsorption in natural systems will require information on the growth phase of the population. However, in most natural environments, nutrient limitation and predation should make exponential-phase cells rare. As a first approximation then, model parameters from either stationary or sporulated phase may be applied to most natural environments. Second, we point out that the results of this study apply only to resting cells. Urrutia et al. (1992) and Kemper et al. (1993) have shown that a membrane-induced proton motive force continuously supplies H^+ to the wall of metabolically active cells, and as a result, they may adsorb less metal from solution than resting cells. In addition, metabolically active bacteria may produce extracellular polysaccharides or metabolites that affect metal adsorption. Although much recent work has clarified the relationship between metal adsorption and abiotic variables (such as pH and ionic strength), our knowledge of the effects of biotic variables is, at present, limited.

Acknowledgments—This research was supported by an Natural Sciences and Engineering Research Council of Canada (NSERC) operating grant to D. Fortin. We thank D. Scott Smith and F. Grant Ferris for helpful discussions, and we thank X. Châtellier for reviewing an early version of this manuscript. This manuscript was greatly improved by the reviews of Lesley Warren and two anonymous reviewers.

Associate editor: N. E. Ostrom

REFERENCES

Baes C. F. and Mesmer R. E. (1976) *The Hydrolysis of Cations*. Wiley.

Baker E. T., Freely R. A., Mottl M. J., Sansone F. T., Wheat C. G., Resing J. A., and Lupton J. E. (1994) Hydrothermal plumes along the East Pacific Rise, 8°40′ to 11°40′N: Plume distribution and relationship to the apparent magmatic budget. *Earth Planet. Sci. Lett.* **128,** 1–17.

Baughman G. L. and Paris D. F. (1981) Microbial bioconcentration of organic pollutants from aquatic systems—critical review. *Crit. Rev. Microbiol.* **8,** 205–228.

Beveridge T. J. (1989) Role of cellular design in bacterial metal accumulation and mineralization. *Annu. Rev. Microbiol.* **43,** 147–171.

Beveridge T. J., Forsberg C. W., and Doyle R. J. (1982) Major sites of metal binding in *Bacillus licheniformis* walls. *J. Bacteriol.* **150,** 1438–1448.

Beveridge T. J., Meloche J. D., Fyfe W. S., and Murray R. G. E. (1983) Diagenesis of metals chemically complexed to bacteria: laboratory formation of metal phosphates, sulfides, and organic condensates in artificial sediments. *Appl. Env. Microb.* **45,** 1094–1108.

Beveridge T. J. and Murray R. G. E. (1980) Sites of metal deposition on the cell wall of *Bacillus subtilis*. *J. Bacteriol.* **141,** 876–887.

Butter T. J., Evison L. M., Hancock I. C., Holland F. S., Matis K. A., Philipson A., Sheikh A. I., and Zouboulis A. I. (1998) The removal and recovery of cadmium from dilute aqueous solutions by biosorption and electrolysis at laboratory scale. *Wat. Res.* **32,** 400–406.

Chang J.-O., Law R., and Chang C.-C. (1997) Biosorption of lead, copper and cadmium by biomass of *Pseudomonas aeruginosa* PU21. *Wat. Res.* **31,** 1651–1658.

Chapelle F. H. (1993) *Ground-Water Microbiology and Geochemistry*. Wiley.

Corapcioglu M. Y. and Kim S. (1995) Modeling facilitated contaminant transport by mobile bacteria. *Wat. Res.* **31,** 2693–2647.

Cox J. S., Smith D. S., Warren L. A., and Ferris F. G. (1999) Characterizing heterogenous bacterial surface functional groups using discrete affinity spectra for proton binding. *Env. Sci. Tech.* **33,** 4514–4521.

Daughney C. J. and Fein J. B. (1998a) The effect of ionic strength on the adsorption of H^+, Cd^{2+}, Pb^{2+} and Cu^{2+} by *Bacillus subtilis* and *Bacillus licheniformis*: A surface complexation model. *J. Coll. Interface Sci.* **198,** 53–77.

Daughney C. J. and Fein J. B. (1998b) Sorption of 2,4,6-trichlorophenol by *Bacillus subtilis*. *Env. Sci. Tech.* **32,** 749–752.

Daughney C. J., Fein J. B., and Yee N. (1998) A comparison of the thermodynamics of metal adsorption onto two common bacteria. *Chem. Geol.* **144,** 161–176.

Fein J. B. and Delea D. (1999) Experimental study of the effect of EDTA on Cd adsorption by *Bacillus subtilis*: a test of the chemical equilibrium approach. *Chem. Geol.* **161,** 375–383.

Fein J. B., Daughney C. J., Yee N., and Davis T. (1997) A chemical equilibrium model for metal adsorption onto bacterial surfaces. *Geochim. Cosmochim. Acta* **61,** 3319–3328.

Fortin D., Ferris F. G., and Beveridge T. J. (1997) Surface-mediated mineral development by bacteria. In *Geomicrobiology: Interactions Between Microbes and Minerals* (eds. J. F. Banfield and K. H. Nealson), *Reviews in Mineralogy* **35,** pp. 391–428, Mineralogical Society of America, Washington, DC.

Fortin D. and Ferris F. G. (1998) Precipitation of iron, silica and sulfate on bacterial cell surfaces. *Geomicrobiol. J.* **15,** 309–324.

Fowle D. A. and Fein J. B. (1999) Competitive adsorption of metal cations onto two gram positive bacteria: Testing the chemical equilibrium model. *Geochim. Cosmochim. Acta* **63,** 3059–3067.

Fowle D. A. and Fein J. B. (2000) Experimental measurements of the reversibility of metal-bacteria adsorption reactions. *Chem. Geol.* **168,** 27–36.

Fowle D. A., Fein J. B., and Martin A. M. (2000) Experimental study of uranyl adsorption by *Bacillus subtilis*. *Environ. Sci. Tech.* **34,** 3737–3741.

Friis N. and Meyers–Keith P. (1986) Biosorption of uranium and lead by *Streptomyces longwoodensis*. *Biotech. Bioeng.* **28,** 21–28.

Gadd G. M. (1988) Accumulation of metals by microorganisms and algae. In *Biotechnology* (eds. H.-J. Rehm and G. Reed), Vol. 6B, pp. 401–433. VCH Publishers.

Geesey G. G., Richardson W. T., Yeomans H. G., Irvin R. T., and Costerton J. W. (1977) Microscopic examination of natural sessile bacterial populations from an alpine stream. *Can. J. Microbiol.* **23,** 1733–1736.

Ghiorse W. S. and Wobber F. J. (1989) *Deep Subsurface Microbiology*. Geomicrobiology J., 7. Crane, Russak & Co.

Gonçalves M. L. S., Sigg L., Reutlinger M., and Stumm W. (1987) Metal ion binding by biological surfaces: Voltametric assessment in the presence of bacteria. *Sci. Tot. Environ.* **60,** 105–119.

Harvey R. W., Lion L. W., Young L. Y., and Leckie J. O. (1982) Enrichment and association of lead and bacteria at particulate surfaces in a salt-marsh surface layer. *J. Marine Res.* **40,** 1201–1211.

Kemper M. A., Urrutia M. M., Beveridge T. J., Koch A. K., and Doyle R. J. (1993) Proton motive force may regulate cell wall-associated enzymes of *Bacillus subtilis*. *J. Bacteriol.* **175,** 5690–5696.

Kjelleberg S. and Hermansson M. (1984) Starvation-induced effects on bacterial surface characteristics. *Appl. Env. Microb.* **48,** 497–503.

Konhauser K. O., Fyfe W. S., Ferris F. G., and Beveridge T. J. (1993) Metal sorption and precipitation by bacteria in two Amazonian river systems: Rio Solimoes and Rio Negro, Brazil. *Geology* **21,** 1103–1106.

Kushner D. J. (1978) *Microbial Life in Extreme Environments*. Academic Press.

Langmuir D. (1997) *Aqueous Environmental Geochemistry*. Prentice-Hall.

Macaskie L. E. and Dean A. C. R. (1984) Cadmium accumulation by a *Citrobacter* sp. *J. Gen. Microb.* **130,** 53–62.

Mahmood S. K. and Rama R. P. (1993) Microbial abundance and degradation of polycyclic aromatic hydrocarbons in soil. *Bull. Environ. Contam. Toxicol.* **50,** 486–491.

Mandernack K. W. and Tebo B. M. (1993) Manganese scavenging and oxidation at hydrothermal vents and in vent plumes. *Geochim. Cosmochim. Acta* **57,** 3907–3923.

Marshall K. C. (1980) Adsorption of microorganisms to soils and sediments. In *Adsorption of Microorganisms to Surfaces* (eds. G. Bitton and K. C. Marshall), pp. 317–329. John Wiley and Sons.

Martell A. E. and Smith R. M. (1977) *Critical Stability Constants. III: Other Organic Ligands*. Plenum Press.

McEldowney S. and Fletcher M. (1986) Effect of growth conditions and surface characteristics of aquatic bacteria on their attachment to solid surfaces. *J. Gen. Microb.* **132,** 513–523.

McLean R. J. C. and Beveridge T. J. (1990) Metal-binding capacity of bacterial surfaces and their ability to form mineralized aggregates. In *Microbial Mineral Recovery* (eds. H. L. Erlich and C. L. Brierly), pp. 185–222. McGraw Hill Publishing.

Norberg A. B. and Persson H. (1984) Accumulation of heavy-metal ions by *Zoogloea ramigera*. *Biotech. Bioeng.* **26,** 239–246.

Savvichev A. S., Nikitin D. I., and Oranskaya M. S. (1986) The two phases of colloidal gold accumulation by immobilized microorganisms. *Geochem. Int.* **23,** 60–62.

Shuttleworth K. L. and Unz R. F. (1993) Sorption of filamentous bacterium *Thiothrix* strain A1. *Appl. Env. Microb.* **59,** 1274–1282.

Smith R. M. and Martell A. E. (1976) *Critical Stability Constants. IV: Inorganic Complexes*. Plenum Press.

Stenström T. A. (1989) Bacterial hydrophobicity, an overall parameter for the measurement of adhesion potential to soil particles. *Appl. Env. Microb.* **55,** 142–147.

Stenström T. A. and Kjelleberg S. (1985) Fimbriae mediated nonspecific adhesion of *Salmonella typhimurium* to mineral particles. *Arch. Microb.* **143,** 6–10.

Tortora G. J., Funke B. R., and Case C. L. (1995) *Microbiology*, 5th Ed. Benjamin-Cummings Publ. Co.

Urrutia M. M., Kemper M., Doyle R. J., and Beveridge T. J. (1992) The membrane-induced proton motive force influences the metal binding ability of *B. subtilis* cell walls. *Appl. Env. Microb.* **58,** 3837–3844.

van Loosdrecht M. C. M., Lyklema J., Norde W., and Zehnder A. J. B. (1989) Bacterial adhesion: a physicochemical approach. *Microb. Ecol.* **17,** 1–15.

van Loosdrecht M. C. M., Lyklema J., Norde W., and Zehnder A. J. B. (1990) Hydrophobic and electrostatic parameters in bacterial adhesion. *Aquat. Sci.* **52,** 103–113.

Volesky B. and Holan Z. R. (1995) Biosorption of heavy metals. *Biotech. Prog.* **11,** 235–250.

Warren L. A. and Ferris F. G. (1998) Continuum between sorption and precipitation of Fe(III) on microbial surfaces. *Env. Sci. Tech.* **32,** 2331–2337.

Weiss T. H., Mills A. L., Hornberger G. M., and Herman J. S. (1995) Effect of bacterial cell chape on transport of bacteria in porous media. *Env. Sci. Tech.* **29,** 1737–1740.

Westall J. C. (1982a) FITEQL: A computer program for the determination of chemical equilibrium constants from experimental data: Version 1.2, Report 82-01. Department of Chemistry, Oregon State Univ.

Westall J. C. (1982b) FITEQL: A computer program for the determination of chemical equilibrium constants from experimental data: Version 1.2, Report 82-02. Department of Chemistry, Oregon State Univ.

Yakimov M. M., Timmis K. N., Wray V., and Fredrickson H. L. (1995) Characterization of a new lipopeptide surfactant produced by therotolerant and halotolerant subsurface *Bacillus licheniformis* BA S50. *Appl. Env. Microbiol.* **61,** 1706–1713.

Yee N., Fein J. B., and Daughney C. J. (2000) Experimental study of the pH, ionic strength, and reversibility behavior of bacteria-mineral adsorption. *Geochim. Cosmochim. Acta* **64,** 609–617.